12-28-2022

Decadal Time-Series Depletion of Dissolved Oxygen at Abyssal Depths in the Northeast Pacific

K. L. Smith
Monterey Bay Aquarium Research Institute

M. Messié
Monterey Bay Aquarium Research Institute

T. P. Connolly
San Jose State University, thomas.p.connolly@sjsu.edu

C. L. Huffard
Monterey Bay Aquarium Research Institute

Geophysical Research Letters®

Key Points:

- Oxygen concentration has significantly declined in abyssal waters of the NE Pacific over 30 years
- Oxygen concentration in the NE Pacific correlates with physical and biological conditions from the surface ocean to the seafloor

Correspondence to:

K. L. Smith Jr.,
ksmith@mbari.org

Author Contributions:

Conceptualization: K. L. Smith
Data curation: M. Messié, T. P. Connolly, C. L. Huffard
Formal analysis: M. Messié, T. P. Connolly, C. L. Huffard
Funding acquisition: K. L. Smith
Investigation: K. L. Smith
Methodology: M. Messié, T. P. Connolly, C. L. Huffard
Project Administration: K. L. Smith
Resources: K. L. Smith
Supervision: K. L. Smith
Visualization: K. L. Smith
Writing – original draft: K. L. Smith
Writing – review & editing: K. L. Smith, M. Messié, T. P. Connolly, C. L. Huffard

Decadal Time-Series Depletion of Dissolved Oxygen at Abyssal Depths in the Northeast Pacific

K. L. Smith Jr.[1] , **M. Messié**[1] , **T. P. Connolly**[2] , and **C. L. Huffard**[1]

[1]Monterey Bay Aquarium Research Institute, Moss Landing, CA, USA, [2]Moss Landing Marine Laboratories, San José State University, Moss Landing, CA, USA

Abstract Dissolved oxygen depletion in the global ocean is well documented over several decades from the surface ocean to abyssal depths. This decline is especially prevalent in the Northeast Pacific. A significant decline in dissolved oxygen has been measured over 30 years at 4,000–4,100 m depth (Station M) beneath the California Current off central California. Three principal hypotheses examined the relationship of declining oxygen with biological and physical factors over the 30-year time series. Annual resolution revealed Ekman pumping, coastal upwelling, particulate matter flux, and sediment community oxygen consumption having significant correlations with bottom water dissolved oxygen concentration. Coastal upwelling accounted for 65% of the annual variation in bottom water oxygen concentration. Stepwise regression yielded descriptive models of bottom water dissolved oxygen using coastal upwelling, wind stress and primary production variables. Is continued oxygen depletion in the Northeast Pacific indicative of abyssal regions in the world ocean?

Plain Language Summary The dissolved oxygen content of the global ocean has been declining over many decades. This decrease is well documented in the upper ocean particularly in the Northeast Pacific Ocean. To examine the change in dissolved oxygen at greater depths, we measured the bottom water oxygen concentration at 4,000–4,100 m depth at a single station in the Northeast Pacific over a 30-year period from 1989 through 2019. We recorded a significant decline in dissolved oxygen at this abyssal station over three decades. We then examined possible biological and physical causes of this declining dissolved oxygen. Surface ocean Ekman pumping, coastal upwelling, particulate matter flux, and sediment community oxygen consumption on the seafloor revealed significant relationships with bottom water dissolved oxygen. Coastal upwelling overlying this station accounted for 65% of the annual variation in bottom water oxygen concentration. The question we are now poised to address is whether there is a similar long-term decline in dissolved oxygen concentration at abyssal depths in other regions of the world ocean.

1. Introduction

Dissolved oxygen concentration in the global ocean and coastal waters has been declining over many decades, causing much concern over documented and anticipated impacts on marine ecosystems and biogeochemical cycling (e.g., Breitburg et al., 2018; Helm et al., 2011; Keeling et al., 2010; Schmidtko et al., 2017). This depletion in oxygen is attributed to increasing global temperatures, upper ocean stratification and biological production combined with increasing run-off of nutrients in coastal zones. Hypoxic regions in coastal areas (Chan et al., 2008) and the vertical expansion of the oxygen minimum zones in the Northeast Pacific are well documented (Bograd et al., 2008; Chan et al., 2008; Pierce et al., 2012; Pitcher et al., 2021). In the deep ocean, changes in oxygen concentration can be attributed to biological consumption, advection, surface saturation levels, and age of the water since ventilation. Depletion of oxygen in the deep ocean has been related to reduced exchange with the surface mixed layer allowing more time for biologically mediated utilization. This depletion of dissolved oxygen has been estimated from time-series hydrocast sampling through 2000 (Helm et al., 2011) and analysis of observational databases (Schmidtko et al., 2017). Because of the paucity of time-series measurements of dissolved oxygen below 1,000 m, general ocean circulation models have also been used to estimate deeper water concentrations (e.g., Keeling et al., 2010; Sarmiento et al., 1998).

Oxygen depletion in the California Current has been well documented (e.g., Pitcher et al., 2021). A 16-year time series (1998–2013) along a transect of stations across the central California Current (CalCOFI line 67) showed a significant decline of dissolved oxygen at depths down to 400 m (Ren et al., 2018). This decline can be attributed

to changes in the northward transport of deoxygenated tropical waters in the California Undercurrent (Meinvielle & Johnson, 2013), decadal-scale variability in thermocline depth and respiration in the eastern North Pacific (Deutsch et al., 2011), or periods of reduced ventilation in the western North Pacific (Mecking et al., 2008). A time-series of bottom water dissolved oxygen concentration was measured over a 30-year period (1989–2019) at 4,000–4,100 m depth (Station M), to the south of line 67, showed a significant decrease (Smith et al., 2020). Such a decrease in oxygen at abyssal depths could be influenced by reduction in oceanic overturn and ventilation, and/or increased biological consumption. Changes in oxygen concentration strongly indicate a changing deep-sea ecosystem at Station M. To address the possible reasons for the decline in dissolved oxygen concentration at Station M, we analyzed biological parameters including chlorophyll concentration, primary production, export flux of carbon from the euphotic zone, the flux of particulate material to abyssal depths, the accumulation of phytodetrital matter on the seafloor, and the consumption of oxygen by the sediment community. In addition, physical parameters were examined including temperature, salinity, potential density (σ_θ), wind stress, Ekman pumping and coastal upwelling, the North Pacific Gyre Oscillation (NPGO, Di Lorenzo et al., 2008) and the Pacific Decadal Oscillation (PDO, Mantua & Hare, 2002) over 30 years from 1989 through 2019. Null hypotheses were tested to address whether changes in biological attributes, water mass, surface ocean, and climate conditions in overlying waters may explain the long-term decline in oxygen concentration at abyssal depths at Station M. The three principal null hypotheses with corollary components are listed below:

1. Oxygen depletion in abyssal waters at Station M was not significantly correlated ($p < 0.05$) with biological parameters from 1989 through 2019, specifically:
   a) Chlorophyll concentration (Chl), primary production (PP), and export flux (EF) from the euphotic zone,
   b) Particulate mass or carbon flux between 3,400 and 4,050 m depth,
   c) Detrital aggregate cover on the seafloor between 4,000 and 4,100 m depth,
   d) Oxygen consumption by the sediment community (SCOC) between 4,000 and 4,100 m depth.
2. Oxygen depletion in abyssal waters at Station M was not significantly correlated ($p < 0.05$) with change in water mass as indicated by:
   a) Temperature, salinity and potential density of bottom water.

3. Oxygen depletion in abyssal waters at Station M was not significantly correlated ($p < 0.05$) with climate and surface ocean conditions, specifically:
   a) Wind stress,
   b) Upwelling (Ekman pumping, coastal upwelling),
   c) PDO,
   d) NPGO.

These hypotheses and corollary components were tested at two temporal resolutions, monthly and annual. Monthly means offered the largest sample sizes for interpreting pairwise relationships. However, given the limited temporal resolution of bottom water oxygen measurements (Winkler titrations), comparable data for all variables were only available for a limited number of months. Given the desire to interpret and provide a descriptive model for long-term trends in bottom water dissolved oxygen, analyses were also conducted using annual means.

2. Materials and Methods

2.1. Study Site

Bottom water oxygen samples were collected at the Station M time-series site in the Northeast Pacific (Figure S1 in Supporting Information S1, blue circle), with a bottom depth ranging from ~4,100 m (1989–2005) to ~4,000 m (2006–2019). Station M is located at the base of the Monterey Deep-Sea Fan, chosen to represent an abyssal area with low relief underlying the California Current upwelling region with productive headland plumes of high primary production reaching the area (Smith & Druffel, 1998). Particulate organic carbon and mass fluxes have increased over the past decade of this time-series study, with large episodic events accounting for an increasing fraction of yearly food supply to the abyss (Smith et al., 2018, 2020).

2.2. Physical and Biological Parameters

2.2.1. Bottom Water Dissolved Oxygen

Dissolved oxygen concentration was measured with Winkler titration (Parsons et al., 1984) of bottom water samples collected using Niskin bottles mounted to a human occupied vehicle (HOV *Alvin*), remotely operated vehicles (ROVs *Tiburon* and *Doc Ricketts*), and on CTD rosettes. Water sample data were available for sites in proximity to Station M at approximately 4,000 m depth (Figure S1 in Supporting Information S1) taken during the World Ocean Circulation Experiment (WOCE) in 1991 (Goyet et al., 1997). Oxygen saturation over the time series was calculated using the method outlined by Garcia and Gordon (1992).

2.2.2. Bottom Water Temperature, Salinity and Potential Density

Bottom water temperature, salinity and potential density (σ_θ) values at Station M prior to 1997 were published previously based on reversing thermometers and water samples from Go-Flo bottles (Masiello et al., 1998). Later temperature and salinity values were measured from CTD casts in 2005 and 2006, and remotely operated vehicles during bottom transects (2006–2019). Potential density was calculated using the international one-atm equation of state of seawater (Millero & Poisson, 1981) and potential temperature (Bryden, 1973).

2.2.3. Ocean Color Products

Phytoplankton growth in surface waters and export of that material below the mixed layer are often represented by three satellite data sets: chlorophyll concentration (Chl), primary production (PP), and export flux (EF). Here we used custom products optimized for the California Current (Kahru et al., 2009, 2015, 2020); PP is derived from chlorophyll, sea surface temperature and photosynthetically active radiation using a linear transformation of the Vertically Generalized Production Model by Behrenfeld and Falkowski (1997) and Kahru et al. (2009); and EF is a linear function of PP (Kahru et al., 2020). Monthly data were downloaded from http://spg-satdata.ucsd.edu/CC4km/ and averaged within a 100-km radius around Station M.

2.2.4. Particulate Mass and Organic Carbon Flux

Particulate matter flux was measured from samples collected by sequencing sediment traps (McLane Parflux). Cups were filled with a preservative (mercuric chloride from 1989 to 2009, 3%–5% buffered formalin from 2009 to 2019) prior to deployment at 600 and 50 m above bottom (mab) at Station M. Zooplankton swimmers were manually removed before the samples were freeze-dried, weighed to calculate mass flux, and analyzed for inorganic and total carbon content using a coulometer (UIC) and elemental analyzer (Perkin-Elmer or Exeter Analytical, University of California Santa Barbara Marine Science Institute Analytical Laboratory) respectively. Data from the 600 mab trap were used when available. Gaps in this data set were infilled using the linear relationship between data from the 600 mab and 50 mab traps. Full details of these methods can be found in Baldwin et al. (1998).

2.2.5. Detrital Aggregate Cover

Detrital aggregate cover on the seafloor at Station M was estimated once per day from benthic time-lapse images annotated to identify areas with phytodetritus and gelatinous detritus. The area with optimum lighting (approximately 5 m² of the seafloor) was analyzed. Total detrital aggregate coverage was estimated using a Canadian Grid system (Wakefield & Genin, 1987) and divided by the field of view to yield percent cover. A single observer (KLS) annotated detrital aggregate cover throughout the entire 30-year time series. Full details of these methods can be found in Smith et al. (2018).

2.2.6. Oxygen Consumption by the Seafloor Community

Sediment community oxygen consumption (SCOC) was estimated over the 30-year time series from 2-day respirometry incubations by four different instruments: an autonomous free vehicle grab respirometer, tube core respirometers, the Benthic Rover I, and the Benthic Rover II. Carbon consumption rates were calculated using a respiratory quotient of 0.85 (Smith, 1987). Further details of SCOC measurements at Station M are provided in Smith et al. (2016, 2021).

2.3. Overlying Surface and Climate Conditions

Wind stress, coastal upwelling (Ekman transport), and Ekman pumping were computed from the CCMP wind product v2.0 (Atlas et al., 2011; Wentz et al., 2015), produced by Remote Sensing Systems and available online at https://www.remss.com/measurements/ccmp/. The V2 CCMP processing combines Version-7 RSS radiometer wind speeds, QuikSCAT and ASCAT scatterometer wind vectors, moored buoy wind data, and ERA-Interim model wind fields using a Variational Analysis Method to produce four maps daily of 0.25° gridded vector winds. CCMP wind speeds were averaged daily from 1989 to 2019 and wind stress computed following Large and Pond (1981). Ekman pumping (at each grid cell) and coastal upwelling (at each latitude) were computed from daily wind stress (Messié et al., 2009, 2022) and averaged monthly. Ekman pumping and wind stress were averaged spatially within a 100 km radius circle centered on Station M, and coastal upwelling was averaged between 34.5° and 36.5°N, which roughly represents the latitudinal region most expected to contribute to Station M export flux (Ruhl et al., 2020).

Data and indices representing long-term climate conditions overlying Station M were compiled at the monthly scale from online sources. The PDO index was downloaded from the National Oceanic and Atmospheric Administration (PDO: https://www.ncei.noaa.gov/pub/data/cmb/ersst/v5/index/ersst.v5.pdo.dat) and the NPGO index from http://www.o3d.org/npgo/data/NPGO.txt.

2.4. Data Analysis

Statistical analyses were conducted using R (R Core Team, 2021) in R Studio (R Studio Team, 2022). Figures were generated using "ggOceanMaps" (Vihtakari, 2020) and "ggplot" (Wickham & Wickham, 2016). Spearman's rank correlations were adjusted for autocorrelation using methods outlined in Pyper and Peterman (1999). Stepwise linear regression was conducted using "olsrr" (Hebbali & Hebbali, 2017) and the "all possible" option. Potential density (σ_θ) and detrital aggregate cover did not clearly pass the test for normality ($\alpha < 0.07$) using the Shapiro Wilk test. Transformation ($\log_{10}$) did not achieved normality, so was not used. Potential density (σ_θ) had one extreme value, in 1993 driven by an anomalously low salinity. This extreme value was temporarily removed to assess its influence. This removal did not alter the results, and it was left in the data set for final analyses. Because Chl, PP and EF use many of the same data inputs and are strongly correlated, only primary production was used for stepwise linear regression. The lack of model heteroscedasticity was confirmed using the Breusch-Pagan Lagrange Multiplier test (Breusch & Pagan, 1979).

3. Results

Bottom water oxygen measurements over a 30-year time-series at Station M from 1989 through 2019 were compared with time-series estimates of conditions in the climate, surface waters, and abyssal depths.

3.1. Physical and Biological Parameters

3.1.1. Bottom Water Dissolved Oxygen

Bottom water oxygen at Station M ranged from 144.8 μmol kg^{-1} in the early 1990s decreasing to 126.9 μmol kg^{-1} beginning in 2012 and remaining low through 2019 (Figures 1a and 2a). Bottom water samples taken in proximity to Station M at 4,005–4,156 m depth during the World Ocean Circulation Experiment (Goyet et al., 1997) in 1991 had similar oxygen concentrations to those taken the same year at Station M at 4,100 m. A regression fitted to the bottom water oxygen values showed a significant decrease ($R^2 = 0.526$; $p < 0.002$) over the 30-year time series (Figure 1a). Calculated oxygen saturation exhibited a narrow range from 336.0 to 337.5 μmol kg^{-1} encompassing values calculated from the WOCE stations (Figure 1b).

3.1.2. Bottom Water Temperature, Salinity, and Potential Density

Monthly bottom water temperature ranged between 1.53 and 1.47°C with a mean of 1.50 ± 0.013 exhibiting no significant change over the time series ($R^2 = 0.011$; $p = 0.59$) (Figure 1c). Similarly, bottom water salinity showed no significant change over the time series ($R^2 = 0.077$; $p = 0.14$) (Figure 1d). Potential density (σ_θ) (Figure 1e) associated with bottom water oxygen measurements at Station M was generally stable throughout the full time
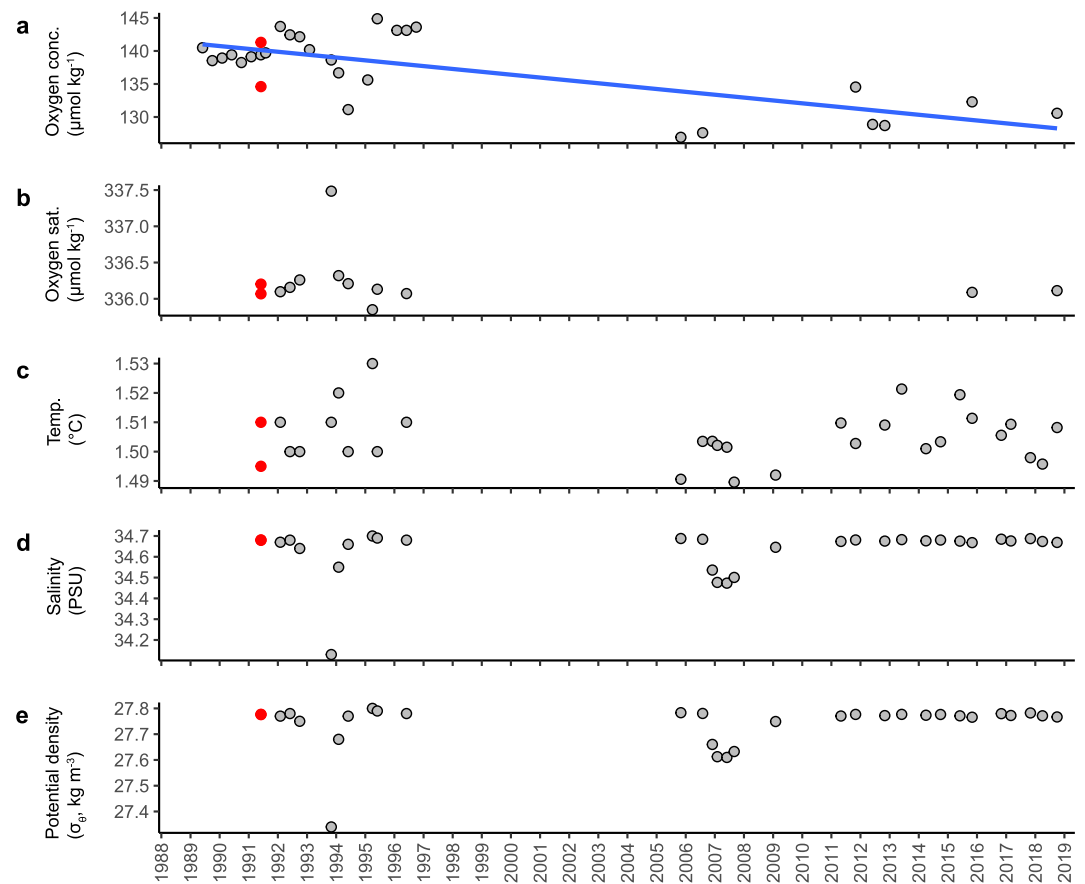
Figure 1. Bottom water conditions at Station M (averaged monthly) and nearby WOCE stations (red dots; Goyet et al., 1997) (a) Oxygen concentrations with linear regression (blue line), (b) oxygen saturation, (c) temperature, (d) salinity, and (e) potential density (σ_θ; Temperature, salinity, and potential density values prior to 1997 were published in Masiello et al. [1998]).

series except for periods of lower values in November 1993 (27.34 kg m^{-3}), February 1994 (27.68 kg m^{-3}), and December 2006 through September 2007 (27.61–27.67 kg m^{-3}). Other than those periods, σ_θ values were consistently between 27.7 kg m^{-3} and 27.8 kg m^{-3} with an average of 27.77 $\pm$ 0.093 kg m^{-3} ($R^2 = 0.06$; $p = 0.19$) (Figure 1e). The consistent values for bottom water temperature, salinity and potential density indicate the same water mass was sampled throughout the time series.

3.1.3. Ocean Color Products

Chlorophyll concentration (Chl) exhibited a consistent seasonal signal with highs in the late fall through early spring (Figure 2b). The monthly mean Chl was 0.5 $\pm$ 0.2 mg C m^{-3} over the time series, peaking at 1.6 mg m^{-3} in August 2018. Chl was generally low in 2014 through 2016, though the lowest value was in April 2019 (0.2 mg^{-3}). Primary production (PP) and export flux (EF, which was calculated from primary production) exhibited a consistent seasonal signal with highs in the spring and summer (Figure 2c). Low values were evident between late 2014 and 2017, with a high peak in August 2018 (PP: 1296.7 mg C m^{-2}d^{-1} EF: 425.2 mg C m^{-2}d^{-1}). The monthly mean primary production over the time series was 538.9 $\pm$ 149.2 mg C m^{-2}d^{-1}, while export flux averaged 123.5 $\pm$ 40.6 mg C m^{-2}d^{-1}.

3.1.4. Particulate Mass and Organic Carbon Flux

Total mass flux exhibited strong seasonal and inter-annual variability ranging from a high of 498.9 mg m^{-2} d^{-1} down to 0.82 mg m^{-2}d^{-1} over the time series (Figure 2d). A similar pattern was observed in particulate organic carbon (POC) flux with monthly ranges from 0.34 to a high of 37.24 mg C m^{-2}d^{-1} over the time series with a
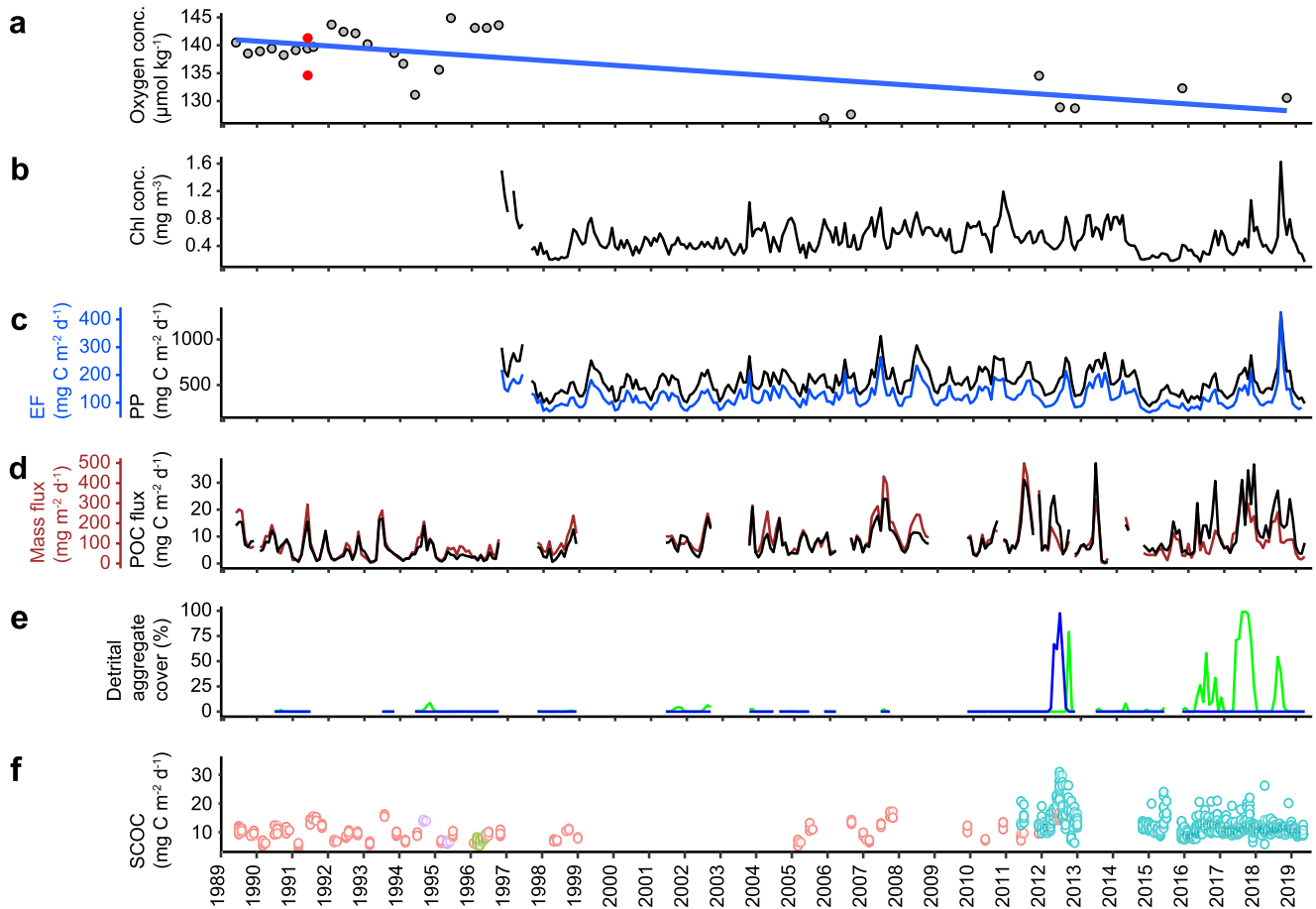
Figure 2. Time series of (a) monthly oxygen concentration at Station M (gray circles) and WOCE stations (red dots; Goyet et al., 1997), along with biological conditions: (b) monthly chlorophyll (Chl) concentration, (c) monthly primary production (PP, black) and export flux (EF, blue), (d) monthly particulate organic carbon (black) and mass flux (brown), (e) monthly detrital aggregate cover of the seafloor (blue = gelatinous detritus, green = phytodetritus), (f) sediment community oxygen consumption (SCOC) daily averages measured by the free vehicle grab respirometer (pink circles), tube core respirometers (purple circles), Benthic Rover I (green circles) and Benthic Rover II (blue circles).

mean of 8.35 ± 6.68 mg C m^{-2}d^{-1}. Rates rarely peaked seasonally above 20 mg C m^{-2}d^{-1} until frequent highs began in 2011 and persisted through 2019 (Figure 2d).

3.1.5. Phytodetritus Cover on Sea Floor

The percent phytodetritus cover on the seafloor during the time series never exceeded 10% until 2012 when several peaks reached 99.3% (Figure 2e). High percent cover became more frequent beginning in 2016 and extending through 2019. Many of these peaks corresponded with high POC and mass fluxes from 2016 to 2019. The mean percent cover of phytodetritus on the seafloor was $6.1 \pm 18.9\%$ over the time series.

3.1.6. Sediment Community Oxygen Consumption (SCOC)

SCOC measured using four different in situ instruments ranged from 5.6 to 21.15 mg C m^{-2}d^{-1} between 1989 until 2011 (Figure 2f). Beginning in 2011 with more frequent measurements using the Benthic Rover II, there were many peaks in SCOC above 20 mg C m^{-2}d^{-1}, one exceeding 30 mg C m^{-2}d^{-1} in 2012 which corresponded to a high in phytodetritus cover on the seafloor (Figures 2e and 2f). The monthly mean SCOC was 10.9 ± 3.0 mg C m^{-2} d^{-1} over the time series.
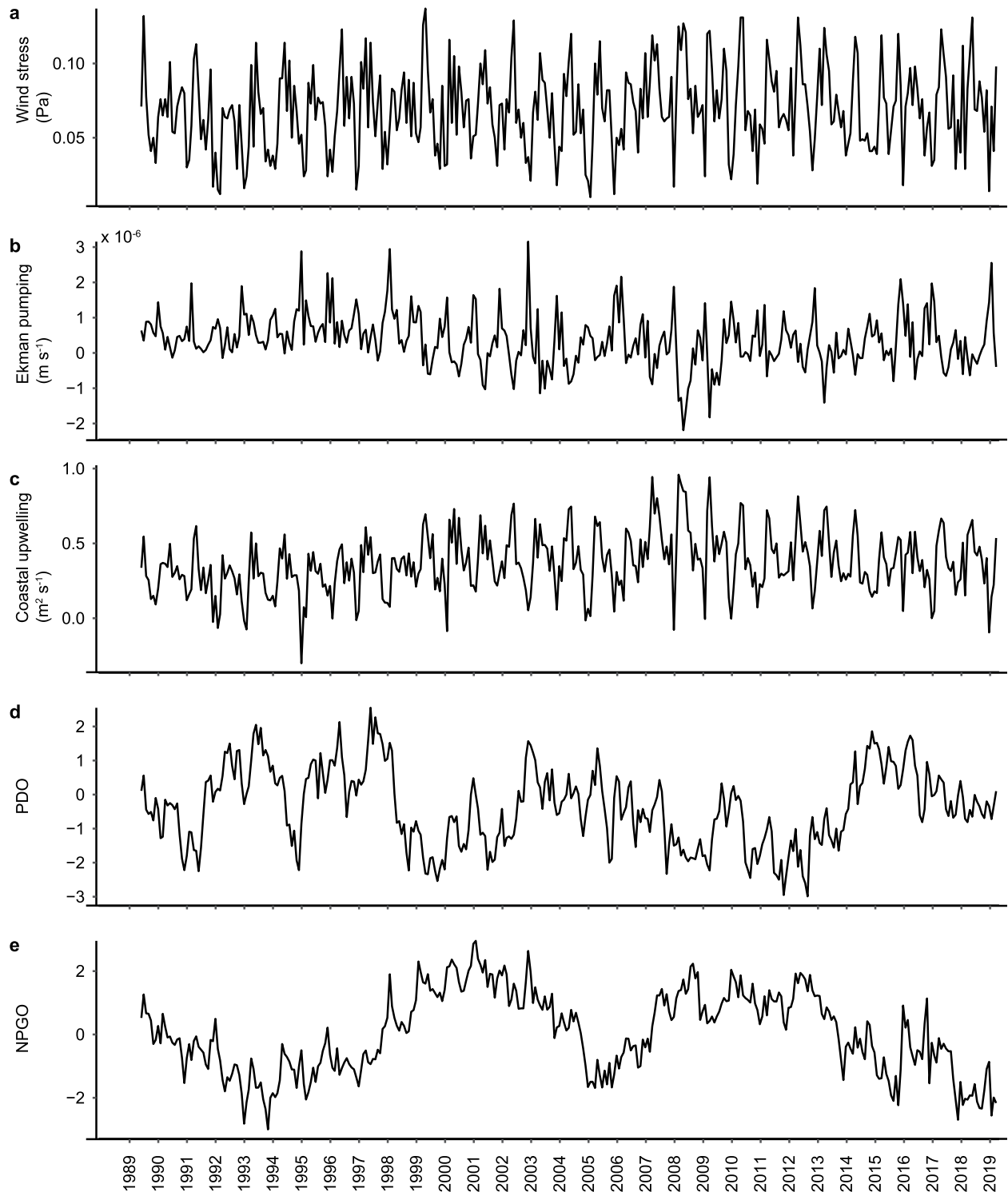
Figure 3. Surface and climate conditions overlying Station M (monthly averages). (a) Wind stress, (b) Ekman pumping, (c) Coastal upwelling, (d) the Pacific Decadal Oscillation (PDO), and (e) the North Pacific Gyre Oscillation (NPGO).

3.2. Overlying Surface and Climate Conditions

Wind stress, Ekman pumping and coastal upwelling showed seasonal highs and lows. Wind stress (Figure 3a) had a monthly mean of 0.07 ± 0.03 Pa, ranging from 0.01 Pa in February 2005 to 0.14 Pa in May 1999. Ekman pumping

Table 1
Correlations Between Bottom Oxygen Concentration ($\mu mol\ kg^{-1}$) and Environmental Conditions at Station M, Aggregated Annually, After Adjustment for Autocorrelation According to Pyper and Peterman (1999)

Environmental condition	Spearman's ρ	P	Degrees of freedom	Adjusted R^2
Biological parameters				
PP	0.464	0.166	4	0.432
EF	0.536	0.121	4	0.357
Chl	0.464	0.169	4	0.632
Mass flux	**−0.503**	**0.050**	**9**	**−0.013**
POC flux	**−0.578**	**0.050**	**7**	**0.178**
Detrital aggregate cover	−0.314	0.181	8	0.081
SCOC	**−0.547**	**0.037**	**9**	**0.247**
Potential density				
Potential density (σ_θ)	0.073	0.416	9	−0.064
Overlying surface and climate conditions				
Station M wind stress	−0.415	0.107	8	0.155
Ekman pumping	**0.547**	**0.050**	**8**	**0.196**
Coastal upwelling	**−0.780**	**0.009**	**6**	**0.646**
PDO index	0.371	0.164	6	0.100
NPGO	0.090	0.419	5	−0.075

Note. Bold indicates $P < 0.05$. Adjusted R^2 is based on a linear model not adjusted for autocorrelation.

(Figure 3b) over Station M averaged $0.35 \pm 0.74 \times 10^{-6}$ m s^{-1}, with a minimum of -2.19 m s^{-1} in May 2008 and a maximum of 3.16 m s^{-1} in December 2002. Coastal upwelling (Figure 3c) averaged 0.36 ± 0.20 m^2 s^{-1}, peaking at 0.96 m^2 s^{-1} in March 2008, and with a low of -0.30 m^2 s^{-1} in January 1995. PDO (Figure 3d) oscillated on multi-year scales, averaging -0.37 ± 1.13, peaking at 2.55 in June 1997, and with a low of -2.99 in September 2012. NPGO averaged 0.03 ± 1.27, and oscillated on decadal scales, with low periods in 1993, 1994, 2005, 2015, and 2018 (lowest approximately -3.0 in November 1993) and peaking in early 2001 at approximately 3.0.

3.3. Relationships Between Parameters: Monthly and Annual Scales

There was only one significant correlation ($p < 0.005$) between bottom water dissolved oxygen and the measured parameters calculated monthly over the time series adjusted for autocorrelation (Table S1 and Figure S2 in Supporting Information S1). PDO was significantly and positively correlated with oxygen concentration ($p = 0.003$). No significant correlations were identified at the monthly scale among the biological (Chl, PP, EF, organic carbon flux, mass flux, detrital aggregate cover, SCOC), potential density (σ_θ), and remaining surface and climate conditions (upwelling).

At the annual scale, Ekman pumping ($p = 0.05$), coastal upwelling ($p = 0.009$), mass flux ($p = 0.05$), POC flux ($p = 0.05$), and SCOC ($p = 0.037$) showed significant correlations with bottom water dissolved oxygen concentration (Table 1, Figure S2 in Supporting Information S1). Coastal upwelling accounted for 65% of the variation ($R^2 = 0.65$) in bottom water oxygen concentration. Like dissolved oxygen concentration, there are significant temporal trends in coastal upwelling (0.0043 m^2 s^{-1} yr^{-1}, $p = 0.014$) and SCOC (0.086 mg C m^{-2} d^{-1} yr^{-1}, $p = 0.021$). A significant correlation between coastal upwelling and bottom water oxygen concentration remains when the temporal trends are removed from each variable (rho $= -0.780$, $p = 0.009$ after adjustment for autocorrelation).

4. Discussion and Conclusions

Results from the 30-year time series at Station M suggest that the observed bottom water oxygen decline from 1989 to 2019 is linked to variability in upwelling-driven carbon export to the deep ocean. At the annual scale, bottom water oxygen concentration was correlated with carbon supply (POC flux) and sediment community oxygen consumption (SCOC), and their key drivers at the surface (Ekman pumping and coastal upwelling). Decadal increases in POC flux (Smith et al., 2018, 2020) and SCOC (Smith et al., 2016) at Station M have coincided with increases in wind stress and upwelling along the California coast (Xiu et al., 2018), trends that are likely to continue with changing climate.

At the monthly time scale, only the PDO correlated significantly. Neither the biological factors examined here, water mass variation (as indicated by σ_θ), nor upwelling explained monthly variation in oxygen concentrations at Station M (Table S1 in Supporting Information S1). This is likely because, unlike the PDO, these variables exhibit strong seasonal variability (Figures 1 and 2). The positive correlation between oxygen concentration and the PDO at the monthly time scale is consistent with relationships observed in the upper ocean from the late 1950s to the early 2000s in the CalCOFI time series (Deutsch et al., 2011). Deutsch et al. (2011) attributed low oxygen during negative phases of the PDO to shoaling of the thermocline, high export flux and high respiration rates in the eastern Pacific. Positive phases of the PDO are associated with the introduction of oxygen rich water into the North Pacific interior (Kwon et al., 2016), but it is unlikely that these processes affect the abyssal depths examined here.

A stepwise linear regression was applied to the annually calculated parameters to generate a descriptive model for bottom water oxygen at Station M over the 30-year time series given the limited data sets. All combinations

Table 2
Summary and Comparison of Oxygen Concentration Decline in the California Current and Northeast Pacific, Adapted From Ren et al. (2018)

References	Potential density (σ_θ)	Depth range (m)	Decline (µmol kg^{-1} year^{-1})	Time period	Region
Bograd et al. (2015)	26.5	0–525	−0.87 to −1.7	1984–2012	S. California Bight
Pierce et al. (2012)	26.3–26.7	0–1000	−0.27 to −0.41	1960s–2000s	Newport Oregon Line
Whitney et al. (2007)	26.3–27	0–4,000	−0.084 to −0.967	1950s–2006	Ocean Station Papa (50°N, 145°W)
Ren et al. (2018)	26.6–26.8	0–800	−1.92	1998–2013	Line 67, Central California
This study	27.3–27.8	4,000–4,100	−0.41	1989–2019	Northeast Pacific Station M

of variables were considered. Based on adjusted R^2 values, the top performing models with two, three and four independent variables respectively were:

Two variables:

$$\text{Oxygen concentration} = 138.27 - 100.32 * \text{Coastal upwelling}$$
$$+ 436.48 * \text{Wind stress} \left(R^2_{\text{adj}} = 0.76, P = < 0.001 \right)$$

Three variables:

$$\text{Oxygen concentration} = 122.25 + 0.006 * \text{PP} - 137.58 * \text{Coastal upwelling}$$
$$+ 814.47 * \text{Wind stress} + \text{PP} \left(R^2_{\text{adj}} = 0.95, P = 0.006 \right)$$

Four variables:

$$\text{Oxygen concentration} = 128.51 - 160.55 * \text{Coastal upwelling} + 876.45 * \text{Wind stress} - 0.94 * \text{PDO}$$
$$+ 0.002 * \text{PP} \left(R^2_{\text{adj}} = 0.98, P = 0.016 \right)$$

These models reinforce the link between coastal upwelling and bottom dissolved oxygen concentrations at abyssal depths at Station M. Coastal upwelling occurs seasonally in the California Current System from Baja California to Washington. Time-series studies in this region have recorded declines in dissolved oxygen from surface waters to depths of 4,100 m over time periods from 1960 to 2019 (Table 2). The declines in dissolved oxygen have ranged from 0.08 up to 1.92 µmol kg^{-1} yr^{-1} with the highest depletion measured along line 67 off the central California coast over a depth range from the surface to 800 m (Ren et al., 2018). The recorded decline at Station M, 4,000–4,100 m depth, over 30 years is comparable to the range measured through the water column during four independent studies (Table 2). The highest declines are recorded at depths shallower than 1,000 m. The only other study in the Northeast Pacific with data at similar abyssal depths is Ocean Station Papa to the northwest (Figure S1 in Supporting Information S1; Table 2), where a smaller decline of −0.08 µmol kg^{-1} yr^{-1} was observed at 4,000 m (Whitney et al., 2007). The larger decline at Station M may be due to the different time period considered and a stronger influence of upwelling-driven primary productivity. Given the regional decline in dissolved oxygen in the Northeast Pacific, the next question is whether this decrease is evident at other abyssal long time-series stations worldwide. This is the subject of our next study.

Conflict of Interest

The authors declare no conflicts of interest relevant to this study.

Data Availability Statement

Supplemental data are available in Zenodo at https://doi.org/10.5281/zenodo.7387248.

References

Atlas, R., Hoffman, R. N., Ardizzone, J., Leidner, S. M., Jusem, J. C., Smith, D. K., & Gombos, D. (2011). A cross-calibrated, multiplatform ocean surface wind velocity product for meteorological and oceanographic applications. *Bulletin of the American Meteorological Society*, *92*(2), 157–174. https://doi.org/10.1175/2010BAMS2946.1

Baldwin, R. J., Glatts, R. C., & Smith, K. L., Jr. (1998). Particulate matter fluxes into the benthic boundary layer at a long time-series station in the abyssal NE Pacific: Composition and fluxes. *Deep Sea Research Part II: Topical Studies in Oceanography*, *45*(4–5), 643–665. https://doi.org/10.1016/s0967-0645(97)00097-0

Behrenfeld, M. J., & Falkowski, P. G. (1997). Photosynthetic rates derived from satellite-based chlorophyll concentration. *Limnology & Oceanography*, *42*(1), 1–20. https://doi.org/10.4319/lo.1997.42.1.0001

Bograd, S. J., Buil, M. P., Di Lorenzo, E., Castro, C. G., Schroeder, I. D., Goericke, R., et al. (2015). Changes in source waters to the Southern California Bight. *Deep Sea Research Part II: Topical Studies in Oceanography*, *112*, 42–52. https://doi.org/10.1016/j.dsr2.2014.04.009

Bograd, S. J., Castro, C. G., Di Lorenzo, E., Palacios, D. M., Bailey, H., Gilly, W., & Chavez, F. P. (2008). Oxygen declines and the shoaling of the hypoxic boundary in the California Current. *Geophysical Research Letters*, *35*(12), L12607. https://doi.org/10.1029/2008gl034185

Breitburg, D., Levin, L. A., Oschlies, A., Grégoire, M., Chavez, F. P., Conley, D. J., et al. (2018). Declining oxygen in the global ocean and coastal waters. *Science*, *359*(6371), eaam7240. https://doi.org/10.1126/science.aam7240

Breusch, T. S., & Pagan, A. R. (1979). A simple test for heteroscedasticity and random coefficient variation. *Econometrica: Journal of the Econometric Society*, *47*(5), 1287–1294. https://doi.org/10.2307/1911963

Bryden, H. L. (1973). New polynomials for thermal expansion, adiabatic temperature gradient and potential temperature of sea water. *Deep-Sea Research and Oceanographic Abstracts*, *20*(4), 401–408. https://doi.org/10.1016/0011-7471(73)90063-6

Chan, F., Barth, J. A., Lubchenco, J., Kirincich, A., Weeks, H., Peterson, W. T., & Menge, B. A. (2008). Emergence of anoxia in the California current large marine ecosystem. *Science*, *319*(5865), 920. https://doi.org/10.1126/science.1149016

Deutsch, C., Brix, H., Ito, T., Frenzel, H., & Thompson, L. (2011). Climate-forced variability of ocean hypoxia. *Science*, *333*(6040), 336–339. https://doi.org/10.1126/science.1202422

Di Lorenzo, E., Schneider, N., Cobb, K. M., Franks, P. J. S., Chhak, K., Miller, A. J., et al. (2008). North Pacific Gyre Oscillation links ocean climate and ecosystem change. *Geophysical Research Letters*, *35*(8), L08607. https://doi.org/10.1029/2007gl032838

Garcia, H. E., & Gordon, L. I. (1992). Oxygen solubility in seawater: Better fitting equations. *Limnology & Oceanography*, *37*(6), 1307–1312. https://doi.org/10.4319/lo.1992.37.6.1307

Goyet, C., Key, R. M., Sullivan, K. F., & Tsuchiya, M. (1997). *Carbon dioxide, hydrographic, and chemical data obtained during the R/V Thomas Washington Cruise TUNES-1 in the equatorial Pacific Ocean (WOCE Section P17C)*. ORNL/CDIAC-99, NDP-062. Carbon Dioxide Information Analysis Center, Oak Ridge National Laboratory. https://doi.org/10.3334/CDIAC/otg.ndp062

Hebbali, A., & Hebbali, M. A. (2017). Package 'olsrr'. Version 0.5 (p. 3).

Helm, K. P., Bindoff, N. L., & Church, J. A. (2011). Observed decreases in oxygen content of the global ocean. *Geophysical Research Letters*, *38*(23), L23602. https://doi.org/10.1029/2011gl049513

Kahru, M., Goericke, R., Kelly, T. B., & Stukel, M. R. (2020). Satellite estimation of carbon export by sinking particles in the California Current calibrated with sediment trap data. *Deep Sea Research Part II: Topical Studies in Oceanography*, *173*, 104639. https://doi.org/10.1016/j.dsr2.2019.104639

Kahru, M., Kudela, R., Manzano-Sarabia, M., & Mitchell, B. G. (2009). Trends in primary production in the California Current detected with satellite data. *Journal of Geophysical Research*, *114*(C2), C02004. https://doi.org/10.1029/2008jc004979

Kahru, M., Lee, Z., Kudela, R. M., Manzano-Sarabia, M., & Mitchell, B. G. (2015). Multi-satellite time series of inherent optical properties in the California Current. *Deep Sea Research Part II: Topical Studies in Oceanography*, *112*, 91–106. https://doi.org/10.1016/j.dsr2.2013.07.023

Keeling, R. F., Körtzinger, A., & Gruber, N. (2010). Ocean deoxygenation in a warming world. *Annual Reviews of Marine Science*, *2*(1), 199–229. https://doi.org/10.1146/annurev.marine.010908.163855

Kwon, E. Y., Deutsch, C., Xie, S.-P., Schmidtko, S., & Cho, Y.-K. (2016). The North Pacific oxygen uptake rates over the past half century. *Journal of Climate*, *29*(1), 61–76. https://doi.org/10.1175/jcli-d-14-00157.1

Large, W. G., & Pond, S. (1981). Open ocean momentum flux measurements in moderate to strong winds. *Journal of Physical Oceanography*, *11*(3), 324–336. https://doi.org/10.1175/1520-0485(1981)011<0324:oomfmi>2.0.co;2

Mantua, N. J., & Hare, S. R. (2002). The Pacific decadal oscillation. *Journal of Oceanography*, *58*(1), 35–44. https://doi.org/10.1023/a:1015820616384

Masiello, C. A., Druffel, E. R. M., & Bauer, J. E. (1998). Physical controls on dissolved inorganic radiocarbon variability in the California Current. *Deep Sea Research Part II: Topical Studies in Oceanography*, *45*(4–5), 617–642. https://doi.org/10.1016/s0967-0645(97)00096-9

Mecking, S., Langdon, C., Feely, R. A., Sabine, C. L., Deutsch, C. A., & Min, D. H. (2008). Climate variability in the North Pacific thermocline diagnosed from oxygen measurements: An update based on the US CLIVAR/CO$_2$ Repeat Hydrography cruises. *Global Biogeochemical Cycles*, *22*(3). https://doi.org/10.1029/2007gb003101

Meinvielle, M., & Johnson, G. C. (2013). Decadal water-property trends in the California Undercurrent, with implications for ocean acidification. *Journal of Geophysical Research: Oceans*, *118*(12), 6687–6703. https://doi.org/10.1002/2013jc009299

Messié, M., Ledesma, J., Kolber, D. D., Michisaki, R. P., Foley, D. G., & Chavez, F. P. (2009). Potential new production estimates in four eastern boundary upwelling ecosystems. *Progress in Oceanography*, *83*(1–4), 151–158. https://doi.org/10.1016/j.pocean.2009.07.018

Messié, M., Sancho-Gallegos, D. A., Fiechter, J., Santora, J., & Chavez, F. (2022). Satellite-based Lagrangian model reveals how upwelling and oceanic circulation shape krill hotspots in the California Current System. *Frontiers in Marine Science*, *9*, 835813. https://doi.org/10.3389/fmars.2022.835813

Millero, F. J., & Poisson, A. (1981). International one-atmosphere equation of state of seawater. *Deep Sea Research Part A. Oceanographic Research Papers*, *28*(6), 625–629. https://doi.org/10.1016/0198-0149(81)90122-9

Parsons, T. R., Maita, Y., & Lalli, C. M. (1984). *A manual of chemical and biological methods for seawater analysis* (p. 173). Pergamon Press.

Pierce, S. D., Barth, J. A., Shearman, R. K., & Erofeev, A. Y. (2012). Declining oxygen in the Northeast Pacific. *Journal of Physical Oceanography*, *42*(3), 495–501. https://doi.org/10.1175/jpo-d-11-0170.1

Pitcher, G. C., Aguirre-Velarde, A., Breitburg, D., Cardich, J., Carstensen, J., Conley, D. J., et al. (2021). System controls of coastal and open ocean oxygen depletion. *Progress in Oceanography*, *197*, 102613. https://doi.org/10.1016/j.pocean.2021.102613

Pyper, B. J., & Peterman, R. M. (1999). Relationship among adult body length, abundance, and ocean temperature for British Columbia and Alaska sockeye salmon (*Oncorhynchus nerka*), 1967–1997. *Canadian Journal of Fisheries and Aquatic Sciences*, *56*(10), 1716–1720. https://doi.org/10.1139/f99-167

R Core Team. (2021). *R: A language and environment for statistical computing*. R Foundation for Statistical Computing. Retrieved from https://www.R-project.org/

Ren, A. S., Chai, F., Xue, H., Anderson, D. M., & Chavez, F. P. (2018). A sixteen-year decline in dissolved oxygen in the central California Current. *Scientific Reports*, *8*(1), 7290. https://doi.org/10.1038/s41598-018-25341-8

R Studio Team. (2022). RStudio: Integrated development environment for R.

Ruhl, H. A., Bahr, F. L., Henson, S. A., Hosking, W. B., Espinola, B., Kahru, M., et al. (2020). Understanding the remote influences of ocean weather on the episodic pulses of particulate organic carbon flux. *Deep Sea Research Part II: Topical Studies in Oceanography*, *173*, 104741. https://doi.org/10.1016/j.dsr2.2020.104741

Sarmiento, J. L., Hughes, T. M. C., Stouffer, R. J., & Manabe, S. (1998). Simulated response of the ocean carbon cycle to anthropogenic climate warming. *Nature*, *393*(6682), 245–249. https://doi.org/10.1038/30455

Schmidtko, S., Stramma, L., & Visbeck, M. (2017). Decline in global oceanic oxygen content during the past five decades. *Nature*, *542*(7641), 335–339. https://doi.org/10.1038/nature21399

Smith, K. L., Jr. (1987). Food energy supply and demand: A discrepancy between particulate organic carbon flux and sediment community oxygen consumption in the deep ocean. *Limnology & Oceanography*, *32*(1), 201–220. https://doi.org/10.4319/lo.1987.32.1.0201

Smith, K. L., Jr., & Druffel, E. R. M. (1998). Long time-series monitoring of an abyssal site in the NE Pacific: An introduction. *Deep Sea Research Part II: Topical Studies in Oceanography*, *45*(4–5), 573–586. https://doi.org/10.1016/s0967-0645(97)00094-5

Smith, K. L., Jr., Huffard, C. L., & Ruhl, H. A. (2020). Thirty-year time series study at a station in the abyssal NE Pacific: An introduction. *Deep Sea Research Part II: Topical Studies in Oceanography*, *173*, 104764. https://doi.org/10.1016/j.dsr2.2020.104764

Smith, K. L., Jr., Huffard, C. L., Sherman, A. D., & Ruhl, H. A. (2016). Decadal change in sediment community oxygen consumption in the abyssal northeast Pacific. *Aquatic Geochemistry*, *22*(5), 401–417. https://doi.org/10.1007/s10498-016-9293-3

Smith, K. L., Jr., Ruhl, H. A., Huffard, C. L., Messié, M., & Kahru, M. (2018). Episodic organic carbon fluxes from surface ocean to abyssal depths during long-term monitoring in NE Pacific. *Proceedings of the National Academy of Sciences*, *115*(48), 12235–12240. https://doi.org/10.1073/pnas.1814559115

Smith, K. L., Jr., Sherman, A. D., McGill, P. R., Henthorn, R. G., Ferreira, J., Connolly, T. P., & Huffard, C. L. (2021). Abyssal Benthic Rover, an autonomous vehicle for long-term monitoring of deep-ocean processes. *Science Robotics*, *6*(60), eabl4925. https://doi.org/10.1126/scirobotics.abl4925

Vihtakari, M. (2020). ggOceanMaps: Plot data on oceanographic maps using "ggplot2". *R Package Version 0.4* (p. 3).

Wakefield, W. W., & Genin, A. (1987). The use of a Canadian (perspective) grid in deep-sea photography. *Deep Sea Research Part A. Oceanographic Research Papers*, *34*(3), 469–478. https://doi.org/10.1016/0198-0149(87)90148-8

Wentz, F. J., Scott, J., Hoffman, R., Leidner, M., Atlas, R., & Ardizzone, J. (2015). *Remote Sensing Systems Cross-Calibrated Multi-Platform (CCMP) 6-hourly ocean vector wind analysis product on 0.25 deg grid, Version 2.0*. Remote Sensing Systems. Retrieved from www.remss.com/measurements/ccmp

Whitney, F. A., Freeland, H. J., & Robert, M. (2007). Persistently declining oxygen levels in the interior waters of the eastern subarctic Pacific. *Progress in Oceanography*, *75*(2), 179–199. https://doi.org/10.1016/j.pocean.2007.08.007

Wickham, H., & Wickham, M. H. (2016). *ggplot2: Elegant graphics for data analysis*. Springer-Verlag.

Xiu, P., Chai, F., Curchitser, E. N., & Castruccio, F. S. (2018). Future changes in coastal upwelling ecosystems with global warming: The case of the California Current System. *Scientific Reports*, *8*(1), 1–9. https://doi.org/10.1038/s41598-018-21247-7